İSTANBUL UNIVERSITY CERRAHPAŞA

ORIGINAL ARTICLE
Electrica 2023; 23(3): 492-504

Power Quality Alleviation of a Grid-Integrated Photovoltaic System Based on Novel Meta-Heuristic Optimization Technique Using OPAL-RT Real-Time Platform

Bhabasis Mohapatra, Binod Kumar Sahu, Swagat Pati

Department of Electrical Engineering, Siksha O Anusandhan Deemed to be University Institute of Technical Education and Research Faculty, Bhubaneswar, Odisha, India

Cite this article as: B. Mohapatra, B. K. Sahu and S. Pati, "Power quality alleviation of a grid-integrated photovoltaic system based on novel meta-heuristic optimization technique using OPAL-RT real-time platform," *Electrica*, 23(3), 492-504, 2023.

ABSTRACT

The minimization of switching losses and the harmonic distortion of the output current are major challenges in high-power applications. This article validates the application of real-time simulation using Opal Real Time Simulation (OPAL-RT) to investigate the power quality of grid-connected photo voltaic (PV) system. The revamped hysteresis current controller (RHCC) for grid-tied inverter system is used for achieving nearly constant switching frequency, faster current tracking, and proper filtration of current in grid-connected PV systems. A hybrid method, combining arithmetic optimization algorithm and particle swarm optimization, is proposed for the first time in this article. Furthermore, it extracts global optima with less controlling parameters as it balances the exploitation and exploration stages. To improve the inverter's efficiency, the selection of an optimal switching frequency of RHCC plays a crucial role. The selection of switching frequency is considered as a trade-off between minimization of switching losses and reduction of harmonics. The duty cycle and inverter hysteresis bands are considered to be the design variables, whereas the current error and the switching frequency are assumed to be the objective functions to be minimized. The improved arithmetic optimization algorithm technique along with advanced controllers is compared with other algorithms by using Simulink/MATLAB environment and experimental setup.

Index Terms—Arithmetic optimization algorithm (AOA), average switching frequency (ASF), improved arithmetic optimization algorithm (IAOA), OPAL-RT 4510, power quality, revamped hysteresis current controller (RHCC).

I. INTRODUCTION

The renewable energy sources (RESs) have attained an extraordinary role in the 21st century [1]. Twenty-five percent of the world's energy consumption is represented by renewable energies. The huge amount of pollution generated by burning of fossil fuels is the main reason behind the increase in demand of green energy. By 2022, India seek out for installation of 40 000 MW clean energy production from RESs. The reduction in costs of cell production has increased the utilization of photovoltaic (PV) systems [2]. The increase in energy demand has numerous problems such as low power factor, grid instability, and power outage [3]. Voltage source inverters are extensively necessary for the industrial and commercial purpose as they convert the DC current and voltage into AC to be consumed by loads or acquitted into the micro-grid. The output of the inverter should be controlled for providing a steady and smooth sinusoidal waveform to the micro-grid and load [4].

A huge number of stochastic algorithms, known as meta-heuristic algorithms, are proposed in the recent decade in order to prevail over the limitations of classical algorithms. The meta-heuristic algorithms are easier for implementation as they do not require constraint functions and derivatives of objective functions. A competent optimization algorithm known as arithmetic optimization algorithm (AOA) based on the distribution characteristics of the major arithmetic operators in mathematics is presented in [5]. In this article, an improved modification of the AOA technique is proposed by merging particle swarm optimization and AOA, called as improved arithmetic optimization algorithm (IAOA), which is engaged for minimization of switching frequency and current error with duty cycle and hysteresis bands as design variables.

Corresponding author:
Swagat Pati

E-mail:
swagatiter@gmail.com

Received: October 27, 2022

Accepted: January 11, 2023

Publication Date: June 20, 2023

DOI: 10.5152/electrica.2023.0199

The power electronic converters require the presence of appropriate control methods for optimal tracking ability, robust stability, error eradication, and abrupt response. Hysteresis current controllers are used to achieve current control in grid-integrated PV systems due to better dynamics and robustness. An RHCC using optimized hysteresis bands is presented in this article along with a traditional hysteresis current controller (THCC). An RHCC has constant switching frequency features due to which the switching frequency decreases. The switching of the Insulated-Gate Bipolar Transistors (IGBT) occurs when the error current passes through the mid of the hysteresis band, which results in reduced current peaks and current slopes in RHCCs [6].

Perturbation and observation [7], incremental conductance [8], and constant voltage [9] are the most widely used conventional control algorithms in PV systems. However, they have drawbacks such as they are unable to respond to constant environmental changes and to locate the maximum power point (MPP). A variety of artificial intelligence techniques like Support Vector Machines and fuzzy logic are implemented to improve the tracking capability of MPP. The artificial intelligence techniques also suffer from disadvantages, as their performance highly depends on experience in determining membership functions and rules. Meta-heuristic algorithms have been taken into consideration in recent years, particularly to solve complicated problems with several variables and acquire the best solutions. Ant colony optimization (ACO), Cuckoo Search, firefly algorithm, Grey Wolf Optimization (GWO), particle swarm optimization (PSO), whale optimization, Differential Evolution, and ACO are a few examples of algorithms [10].

The key contributions in this work are as follows:

1. Design and implementation of a novel IAOA algorithm for rooftop PV-based micro-grid systems.
2. Application of a THCC and an RHCC in grid-tied PV system.
3. Optimal design of the THCC and RHCC using a novel IAOA algorithm.
4. Power quality improvement in grid-tied PV system by addressing the reduced switching losses.
5. Comparative analysis of novel IAOA algorithm along with THCC and RHCC in MATLAB/Simulink environment as well as using real-time digital simulator OPAL-RT 4510.

The organization of the paper is as follows: The PV module model, proposed methodology, and reference current technique are presented in Section II, followed by analysis of advanced controllers and common benchmark functions in Sections III and IV, respectively. In Section V, the explanation of different algorithms is given. Extensive real-time OPAL-RT results along with the experimental setup of an OPAL-RT digital simulator are presented in Section VI to assess the performance of the proposed technique. Finally, the conclusion is summarized in Section VII.

II. SYSTEM MODELING

A. PV Module Model

The accurate modeling of solar cells improves the performance of the PV system. The PV cell is characterized by a source current I_p, which is proportional to the solar insolation. I_d represents the amount of current in the diode, R_{se} represents the series resistance, R_{sh} represents the shunt resistance, α is diode ideality constant, and V_T represents the maximum thermal voltage [11]. The Shockley equation for a single diode model is as follows:

$$I_{pv} = I_p - I_d\left(exp\left(\frac{V_{pv} + I_{pv}R_{se}}{\alpha V_T}\right) - 1\right) - \left(\frac{V_{pv} + I_{pv}R_{se}}{R_{sh}}\right) \quad (1)$$

B. Proposed Methodology

The typical grid-connected PV system along with optimization and advanced controllers is shown in Fig. 1. It is composed of a single-phase full-bridge inverter with an L-type filter to achieve high-quality DC to AC conversion, PV arrays, and a boost converter with optimized duty cycle. The meta-heuristic algorithms fine-tune the hysteresis bands and duty cycle for optimum switching frequency and total harmonic distortion (THD). This article mainly focuses on the analysis of average switching losses of IGBTs and diodes, as the inductor and capacitor losses are independent of the optimization algorithms. The continuous exposure of the IGBTs to high current and voltage during every turn off and turn on of the device produces the switching losses.

C. Reference Current Technique

The reference current tracking technique is elaborated in [12]. The reference current is estimated by taking the grid voltage into consideration. The scaling factor (α) regularly updates with the change in load. Fig. 2 represents the reference current technique in a grid-tied PV system.

III. ANALYSIS OF ADVANCED CONTROLLERS

A. Traditional Hysteresis Current Controller

A THCC consists of two levels from which the control pulses to the IGBTs are derived in such a way that the transistors S_2 and S_3 switch on or off simultaneously. The transistors S_1 and S_4 are also switched on or off simultaneously, but their switching states are complements of switches S_2 and S_3. The allowable error current is determined by the hysteresis controller bandwidth. The average switching frequency (ASF) can be controlled by the optimized hysteresis bands [13].

B. Revamped Hysteresis Current Controller

Fig. 3 shows the operation of an RHCC scheme. The current error is generated by the difference of the actual current and the reference current and then fed to the RHCC similarly as in THCC. When the error current passes the upper or lower band, the devices get turned on and turned off when the error current changes their sign. The switch S_4 will get turned on if the error current passes the upper hysteresis controller band and the switch S_4 will get turned off when the error current decreases toward zero and happen to be negative. The switch S_1 gets turned on when the current freewheels and passes the lower hysteresis band. The switch S_1 gets turned off when the error current moves toward zero and becomes positive. Similar switching patterns take place in other legs during the control scheme.

Inherently, a lockout delay is provided at each switching pattern when the upper and lower switches of individual legs gets mutually turned off. The current of the respective legs freewheels throughout the inherent lockout delay. As the current freewheels and begins at zero passing of the errors, i.e., not at the lower or upper bands, which results in less current error to hysteresis band as compared to THCC [6].

From Fig. 4,

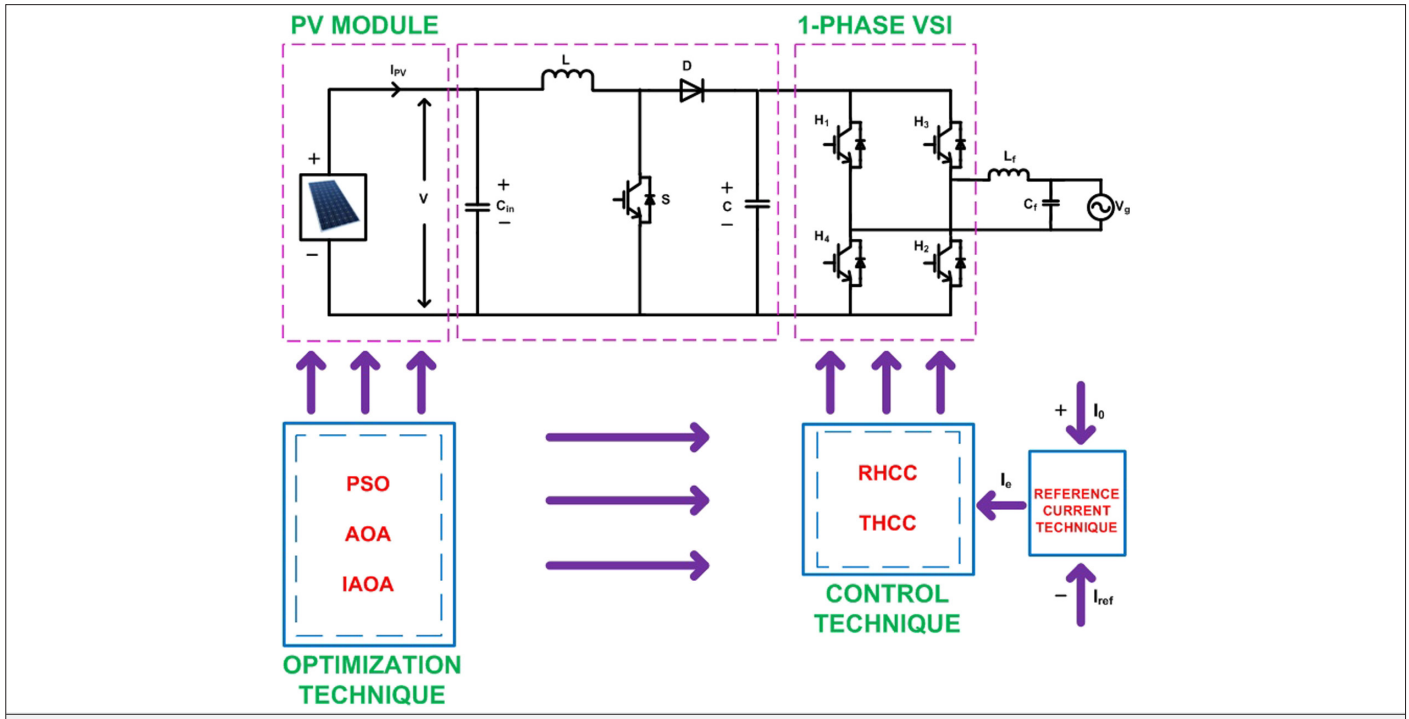

Fig. 1. System block diagram.

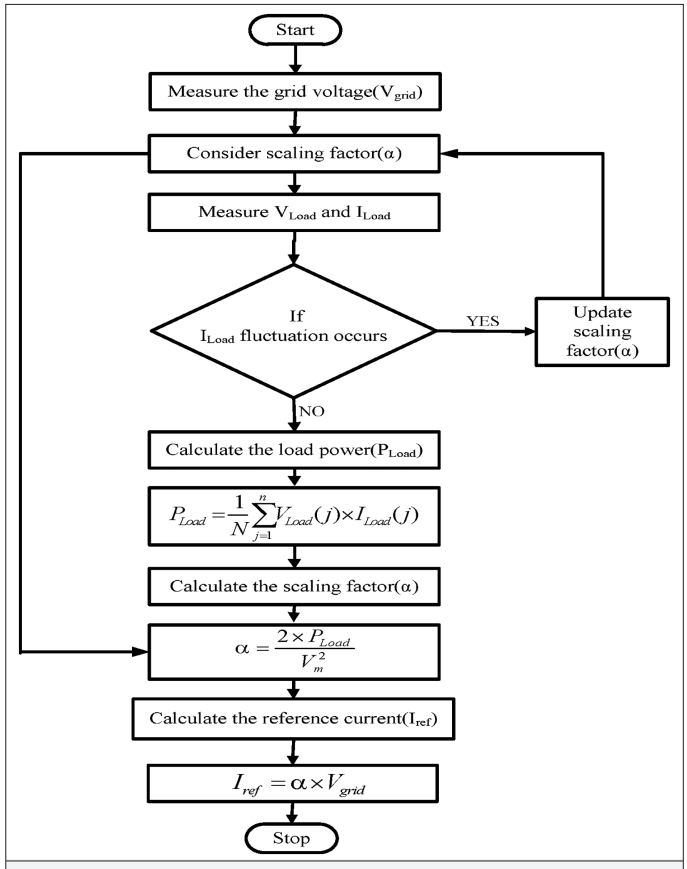

Fig. 2. Reference current technique.

$$error = i_0 - i_{ref} = i_e \tag{2}$$

$$\frac{di_e}{dt} = \frac{V_{DC-}V_g}{L_f} = \frac{\Delta I}{\Delta t} \tag{3}$$

$$\Delta t = \frac{\Delta I L_f}{V_{DC} - V_g} \tag{4}$$

The switching transition period is given by $0 \to t_1 \to T$.

For the cycle $0 \to t_1$

$$\Delta I = 2HB, V_{DC} = +V_{DC}, \Delta t = t_1 \; t_1 = T_{ON} = \frac{2L_f HB}{V_{DC} - V_g} \tag{5}$$

For the cycle $t_1 \to T$

$$\Delta I = -2HB, V_{DC} = -V_{DC}, \Delta t = T - t_1 \; T - t_1 = T_{OFF} = \frac{2L_f HB}{V_{DC} + V_g} \tag{6}$$

The summation of (5) and (6) gives the switching frequency of the RHCC as follows:

$$T = \frac{4L_f HB}{(V_{DC} + V_g)(V_{DC} - V_g)} = \frac{4L_f HB}{V_{DC}^2 - V_g^2} \tag{7}$$

$$f_{s,av}^{RHCC} = \frac{1}{T} = \frac{\left(V_{DC}^2 - V_g^2\right)}{4V_{DC}L_f HB} \tag{8}$$

where $f_{s,av}^{RHCC}$ = ASF of RHCC.

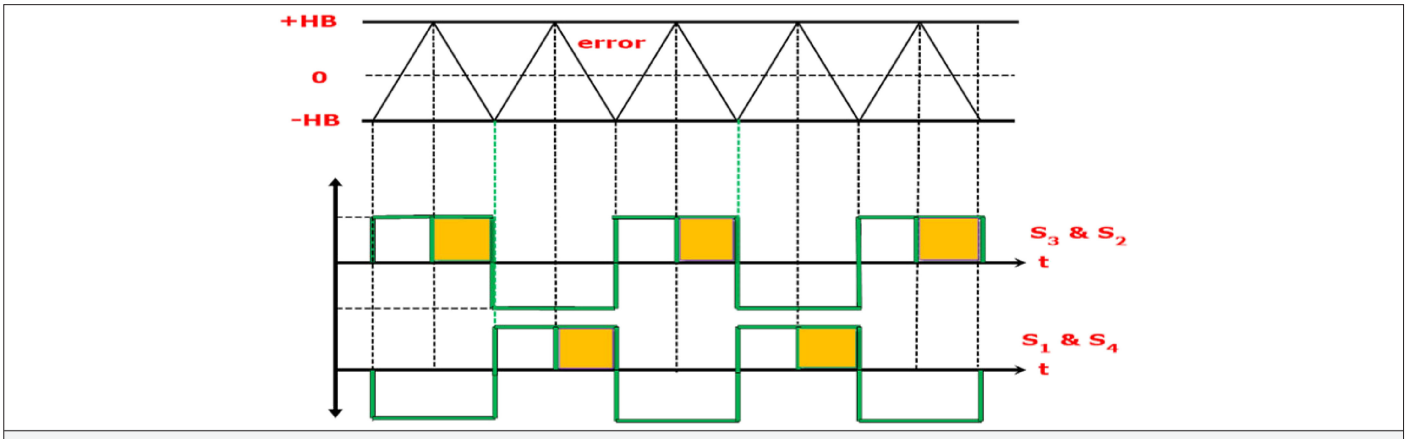

Fig. 3. Analysis of revamped hysteresis current controller.

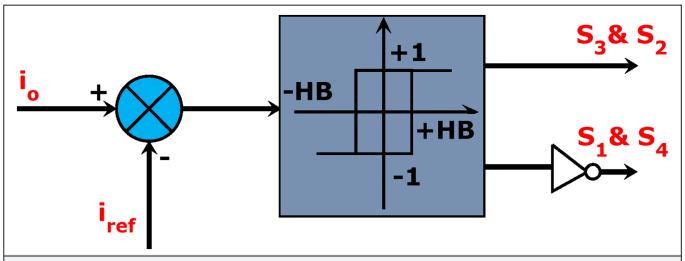

Fig. 4. Switching logic of revamped hysteresis current controller.

IV. COMMON BENCHMARK FUNCTIONS

A set of common standard benchmark functions are chosen to test the efficiency, reliability, and validation of the new optimization technique with variety of problems such as unimodal, separable, and regular. In this article, four standard benchmark functions, namely Levy, Sphere, Rosenbrock, and Michalewicz, are taken into consideration, to test AOA and IAOA algorithms [14]. The function names, their expression, dimension, and ranges are depicted in Table I.

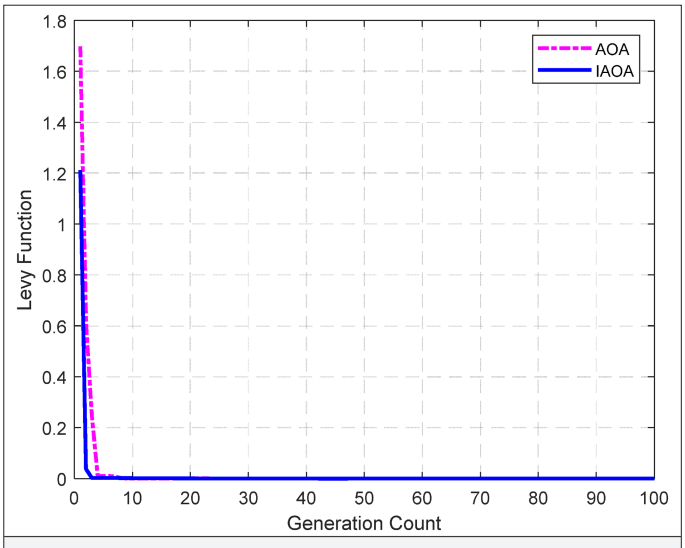

Fig. 5. Convergence characteristics of levy function.

Performance analysis of AOA and IAOA on various benchmark functions is given in Table II.

V. ANALYSIS OF ALGORITHMS

The optimization techniques solve complex problems, characterized by high-performance and multiobjective function handling capability. The combination of two or more optimization techniques thus allows the exploitation of the advantages over the single optimization method [15].

A. Particle Swarm Optimization Algorithm

Particle swarm optimization is derived from the analysis of bird flocking, bees buzzing, and fish schooling. It includes swarms of individuals known as particles. Particles work in social behavior in swarms. At each iteration, the global best of the particles is found by simply adjusting the moving vector according to personal best positions [16].

The steps involved in PSO are elaborated below:

1. Initialization: Within the specific search range, an initial population and initial velocity of size [$NP \times D$] are generated, where "D" is the dimension of the problem and "NP" is the number of population.
2. Velocity updation: Equation (9) is utilized to update the velocity in this step.

$$v_{new} = w \times v_{old} + C_1 \times rand_1 \times \left(p_{best} - x\right) + C_2 \times rand_2 \times \left(g_{best} - x\right) \quad (9)$$

where "C_1" and "C_2" are acceleration constants generally taken as 2.05, p_{best} is the local best, i.e., the best solution so far achieved by a particle, and g_{best} is the global best, i.e., the best solution in the population, $rand_1$ and $rand_2$ are random numbers within the range [0, 1], and "w" is called the inertia weight, which is decreased from 0.9 to 0.4 with iterations.

1. Position updation: Newly generated velocity with the initial population to update the initial population.

$$x_{new} = x_{old} + v_{new} \quad (10)$$

B. Arithmetic Optimization Algorithm

The AOA is a mathematics meta-heuristic algorithm developed in 2021 by Abualigah et al. [14]. Generally, the standard AOA technique has two search spaces such as exploitation and exploration,

TABLE I. DESCRIPTION OF BENCHMARK FUNCTIONS TAKEN IN THE STUDY

Functions	Function's expression	Dimension	Range
Levy	$f(x)=sin^2(\pi\omega_1)+\sum_{i=1}^{d-1}(\omega_i-1)^2\left[1+10sin^2(\pi\omega_i+1)\right]+(\omega_d-1)^2\left[1+sin^2(2\pi\omega_d)\right]$	2	[–10, 10]
Sphere	$f(x)=\sum_{i=1}^{d}x_i^2$	5	[–5.12, 5.12]
Rosenbrock	$f(x)=\sum_{i=1}^{d-1}\left[100\left(x_{i+1}-x_i^2\right)^2+\left(x_i-1\right)^2\right]$	5	[–5, 10]
Michalewicz	$f(x)=-\sum_{i=1}^{d}\sin(x_i)sin^{2m}\left(\frac{ix_i^2}{\pi}\right)$	2	[0, π]

TABLE II. PERFORMANCE ANALYSIS OF AOA AND IAOA ALGORITHMS

Algorithm	Function	Optimum Value	Minimum	Maximum	Mean	Standard Deviation	Computational Time (s)
AOA	F1	0	1.0153×10^{-18}	4.5303×10^{-15}	6.8187×10^{-16}	1.0234×10^{-15}	0.0679
IAOA			1.3498×10^{-31}	1.3498×10^{-31}	1.3498×10^{-31}	6.6809×10^{-47}	0.1173
AOA	F2	0	0	1.4547×10^{-68}	5.2476×10^{-70}	2.6547×10^{-69}	0.0734
IAOA			0	0	0	0	0.1258
AOA	F3	0	6.9507×10^{-05}	7.4774×10^{-04}	3.2929×10^{-04}	1.9981×10^{-04}	0.1400
IAOA			6.8141×10^{-07}	2.9031×10^{-05}	8.6659×10^{-06}	8.0570×10^{-06}	0.2382
AOA	F4	–1.8013	–1.8013	–1.8013	–1.8013	1.1662×10^{-15}	0.0380
IAOA			–1.8013	–1.8013	–1.8013	9.6962×10^{-18}	0.2356

AOA, arithmetic optimization algorithm; IAOA, improved arithmetic optimization algorithm.

motivated by mathematical operations like ÷, ×, +, and – [17]. The basic steps in AOA are as follows:

1. Initialization: During the search process, a dynamic function named math optimizer accelerated (MOA) is employed for switching between exploration and exploitation phases. The following equation defines the MOA function.

$$MOA=min_a+iter\times\left(\frac{max_a-min_a}{iter_{max}}\right) \tag{11}$$

where "*iter*" and "$iter_{max}$" are the iteration count and maximum number of iteration and "min_a" and "max_a" are the minimum and maximum values of the accelerated function taken as 0.2 and 0.9, respectively.

1. Updation phase: Math optimizer probability is denoted as MOP and is calculated using (12).

$$MOP=1-\frac{(iter)^{\frac{1}{\alpha}}}{(iter_{max})^{\frac{1}{\alpha}}} \tag{12}$$

where updation of the solution is done by generating three random numbers r_1, r_2, and r_3 and "α" is taken as 5.

if r_1 < MOA

if r_2 > 0.5, then (exploration phase)

TABLE III. SYSTEM PARAMETERS

Parameter	Numerical Value
Irradiance	500 W/m^2
Line inductance	15 mH
Cell temperature	25°C
Load variation	1000–2000 W
E_{on}	2.2 mJ
E_{off}	1.7 mJ
Grid frequency	50 Hz

TABLE IV. PERFORMANCE ANALYSIS OF VARIOUS CONTROLLERS

Controller	D	HB_1	HB_2	HB_3	HB_4	Max_{SF} (in kHz)	Min_{SF} (in kHz)	Avg_{SF} (in kHz)	Avg_{SFL} (in watts)	Z_{SF} (in kHz)	% THD
PSO–THCC	0.215	0.375	–0.572	–	–	9.25	8.75	7.85	30.60	8.50	0.49
AOA–THCC	0.169	0.620	–0.587	–	–	7.25	3.25	5.50	21.48	6.50	0.57
IAOA–THCC	0.245	0.809	–0.932	–	–	6.25	3.75	5.30	20.67	5.75	0.74
PSO–RHCC	0.490	0.240	0.684	–0.728	–0.884	13.50	9.00	6.46	25.21	7.00	2.06
AOA–RHCC	0.291	0.917	0.753	–0.346	–0.782	10.75	5.75	4.24	16.55	5.50	1.72
IAOA–RHCC	**0.109**	**1.21**	**1.24**	**–1.18**	**–1.19**	**6.50**	**3.25**	**2.53**	**9.88**	**3.50**	**1.05**
Single Band Hysteresis Current Controller (SBHCC) [19]	–	0.5	–0.5	–	–	20	–	–	–	–	4.42
Double Band Hysteresis Current Controller (DBHCC)-1 [19]	–	0.5	–0.5	–	–	10	–	–	–	–	4.33
Double Band Hysteresis Current Controller (DBHCC)-2 [19]	–	0.5	–0.5	–	–	20	–	–	–	–	2.65
ModifiedDouble Band Hysteresis Current Controller (MDBHCC) [19]	–	0.5	–0.5	–	–	5.5	–	–	–	–	4.33
Variable Band Hysteresis Current Controller (VBHCC) [19]	–	0.5	–0.5	–	–	15	–	–	–	–	4.17

AOA, arithmetic optimization algorithm; IAOA, improved arithmetic optimization algorithm; PSO, particle swarm optimization; RHCC, revamped hysteresis current controller; THCC, traditional hysteresis current controller.

$$x_{new} = \frac{g_{best}}{MOP + \varepsilon} \times \left(\left(U_l - L_l \right) \times \mu + L_l \right) \quad (13)$$

else

$$x_{new} = g_{best} \times MOP \times \left(\left(U_l - L_l \right) \times \mu + L_l \right) \quad (14)$$

end

else

if $r_3 < 0.5$ then (exploitation phase)

$$x_{new} = g_{best} - MOP \times \left(\left(U_l - L_l \right) \times \mu + L_l \right) \quad (15)$$

else

$$x_{new} = g_{best} + MOP \times \left(\left(U_l - L_l \right) \times \mu + L_l \right) \quad (16)$$

end

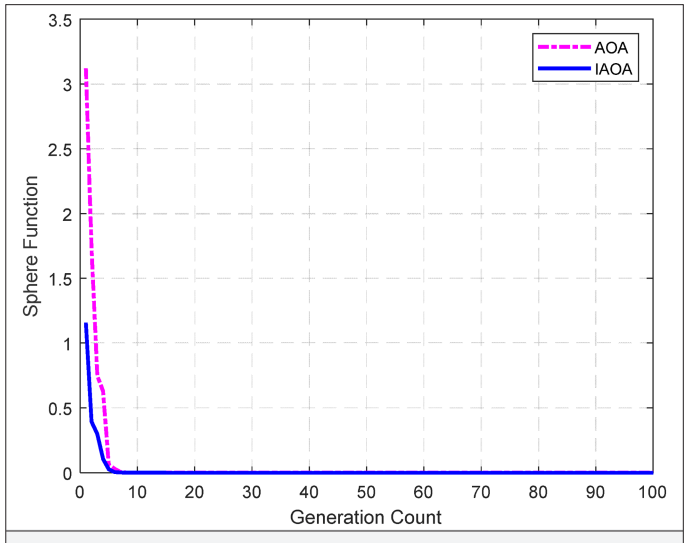

Fig. 6. Convergence characteristics of sphere function.

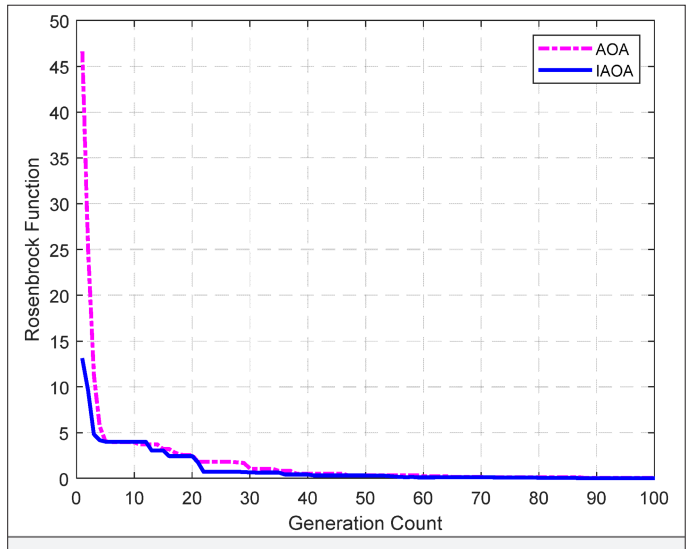

Fig. 7. Convergence characteristics of Rosenbrock function.

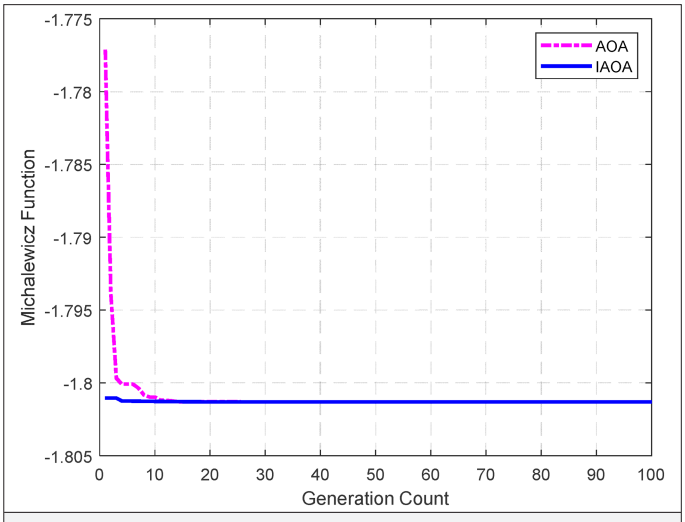

Fig. 8. Convergence characteristics of Michalewicz function.

where "U_1" and "L_1" are the upper and lower limits of the variables to be designed and "α" and "μ" are taken as 5 and 0.5, respectively.

C. Improved Arithmetic Optimization Algorithm

The standard AOA corresponds to a motivating source for exploring the search space. On the other hand, the standard AOA suffers from early stagnation in non-optimal solutions due to poor exploration ability. In contrast to the standard AOA technique, the IAOA technique offers a wider exploration space as each solution is updated with respect to its current position in order to avoid the diversity loss throughout the search process. Furthermore, the AOA technique also faces convergence difficulties as the exploitation phase of standard AOA depends upon the boundaries of design variables. In order to make the exploitation phase stronger, the best performing solution (g_{best}) is generated for movement of solutions in the search space, making it the best-so-far solution than the exploitation phase of the AOA technique. Fig. 9 depicts the flowchart of IAOA. The pseudo-code for the IAOA technique is shown below:

1. Generate the initial population for design variables and the constants "α" and "μ" of the AOA technique.
2. Evaluate the objective function and identify the best performing solution (g_{best}).
3. Update the solution with the AOA technique using (11–16).
4. Update the values of "α" and "μ" with the PSO algorithm using (9 and 10).
5. Repeat the previous two steps until stopping criterion are met.

For optimum switching frequency and THD, the objective function to optimize is shown in (17). Equation (18) shows the average switching losses [18] of the inverter, which majorly includes losses from IGBTs.

$$f = w_1 \times e_i + w_2 \times f_s \tag{17}$$

$$P_{sl} = f_s * mean\left(E_{on} + E_{off}\right) \tag{18}$$

where f_s is the switching frequency, e_i is the current error, and w_1 and w_2 are the weighting factors taken as 0.85 and 0.15, respectively.

VI. RESULTS AND DISCUSSION

The supremacy of the developed model for grid-connected PV system is simulated in MATLAB/SIMULINK environment and then validated in real-time simulator OPAL RT 4510 to obtain the optimum steady state and dynamic response with high power quality. The average switching frequency (Avg_{SF}), average switching losses (Avg_{SFL}), maximum switching frequency (Max_{SF}), minimum

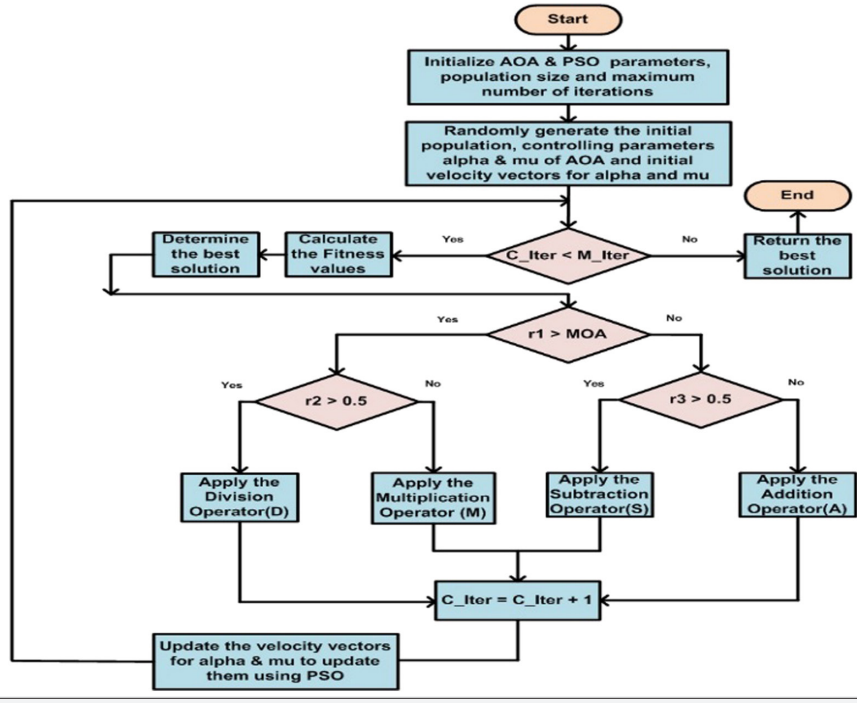

Fig. 9. Flowchart of improved arithmetic optimization algorithm.

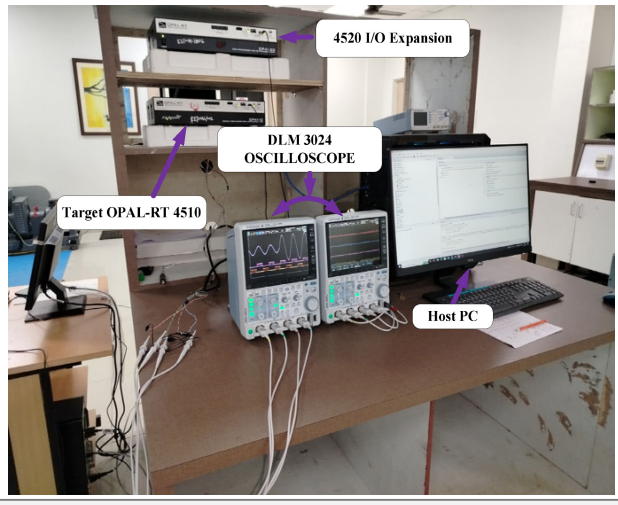

Fig. 10. Experimental setup using OPAL-RT 4510.

switching frequency (Min_{SF}), zero-crossing switching frequency (Z_{SF}), and % THD were obtained using the optimal duty cycle and hysteresis bands selected by PSO–THCC, AOA–THCC, IAOA–THCC, PSO–RHCC, AOA–RHCC, and IAOA–RHCC techniques. In order to analyze the harmonic content present in the output current, power quality analysis has been undertaken. Ultimately, to validate the robustness of the IAOA–RHCC technique, the obtained results are compared with other algorithms with controllers under same working conditions.

Fig. 10 shows the experimental setup consisting of target OPAL-RT 4510, Host PC (view of model/algorithms/control techniques, CPU, and monitor for graphical interface), and DLM3024 Oscilloscope for observation. Figs 11, 12, and 13 elaborate the experimental results of the reference current, actual current, and inverter switching pulses for one cycle for PSO–RHCC, AOA–RHCC, and IAOA–RHCC. The repeated switching of IGBTs and presence of inductors cause unwanted switching losses inside the inverter. The average switching losses are successfully minimized by the proposed IAOA–RHCC scheme.

The actual current is related to the reference current to generate the current error. In a dynamic performance analysis of the PV system with load variations from 1000 W to 2000 W from 4.95 s to 5.05 s, the actual current properly follows the reference current, thereby showing insensitivity to variation in parameters and achieving enhanced global stability. Fig. 14 shows the OPAL-RT-based dynamic performance of the grid-tied PV system with the IAOA–RHCC.

The robustness of the proposed controller, i.e., IAOA–RHCC against variation in output filter inductance and variation in grid voltage, is presented in Fig. 16 and Fig. 17. It can be clearly observed in Fig. 16 that the ASF decreases with increasing output filter inductance in all three cases, i.e., PSO–RHCC, AOA–RHCC, and IAOA–RHCC. But with the proposed control technique (IAOA–RHCC), the deviation of ASF is about 3.19 kHz from minimum to maximum filter inductance, which is recorded to be least in comparison to other two cases. The robustness of the proposed controller toward the grid voltage variation is also proven in Fig. 17. With grid voltage variations of 40%, 80%, 100%, 120%, and 140% of grid voltage, the observation of the average frequencies is taken for all the three above-mentioned cases. The observation shows the deviation in ASF to be least for the proposed control technique (IAOA–RHCC), i.e., about 1.6 kHz. In both the cases, the proposed controller gives the lowest ASF as compared to other two strategies: robustness toward output filter inductance variation and robustness toward grid voltage variation.

The different performance indices with advanced controllers are illustrated in Fig. 18. In comparison to other schemes, the IAOA–RHCC is efficient in reducing the ASF which directly reduces the average switching losses. At that moment, it is possible to accomplish a

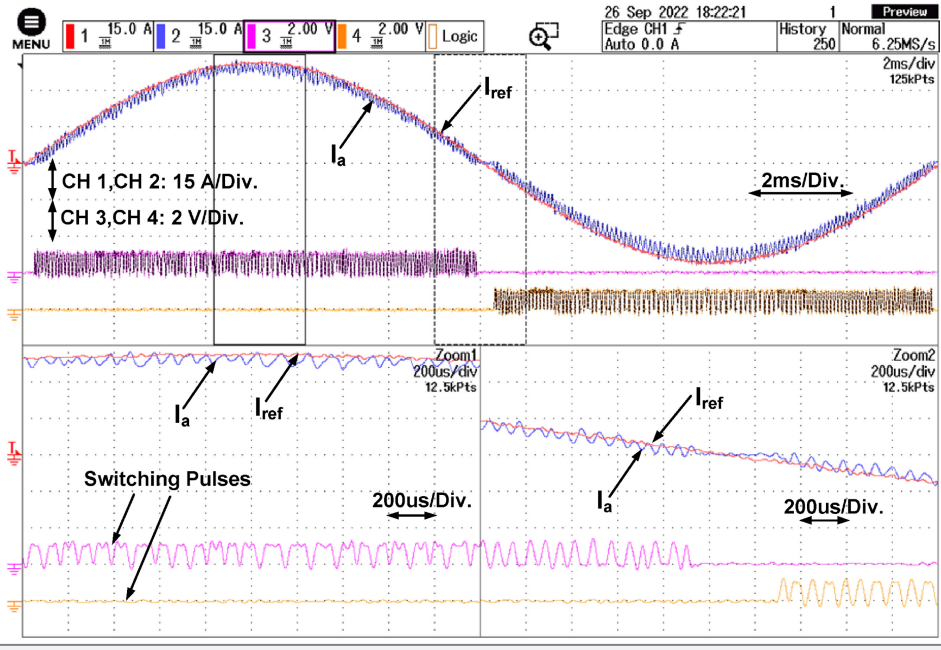

Fig. 11. Experimental results showing I_{ref}, I_a, and switching pulses for particle swarm optimization– revamped hysteresis current controller.

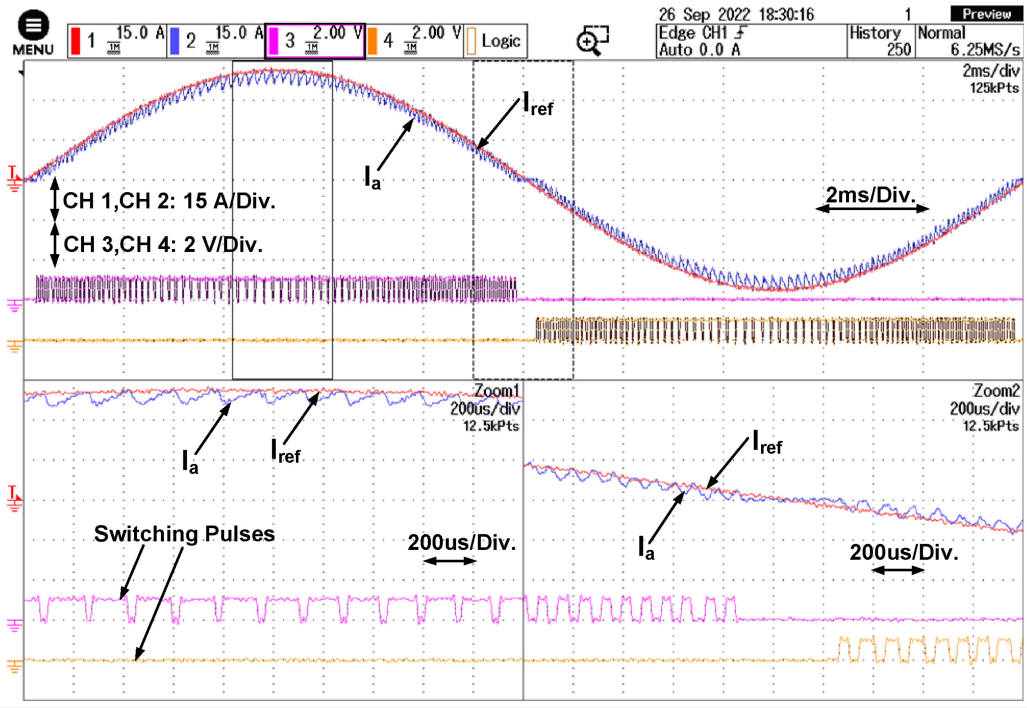

Fig. 12. Experimental results showing I_{ref}, I_a, and switching pulses for arithmetic optimization algorithm–revamped hysteresis current controller.

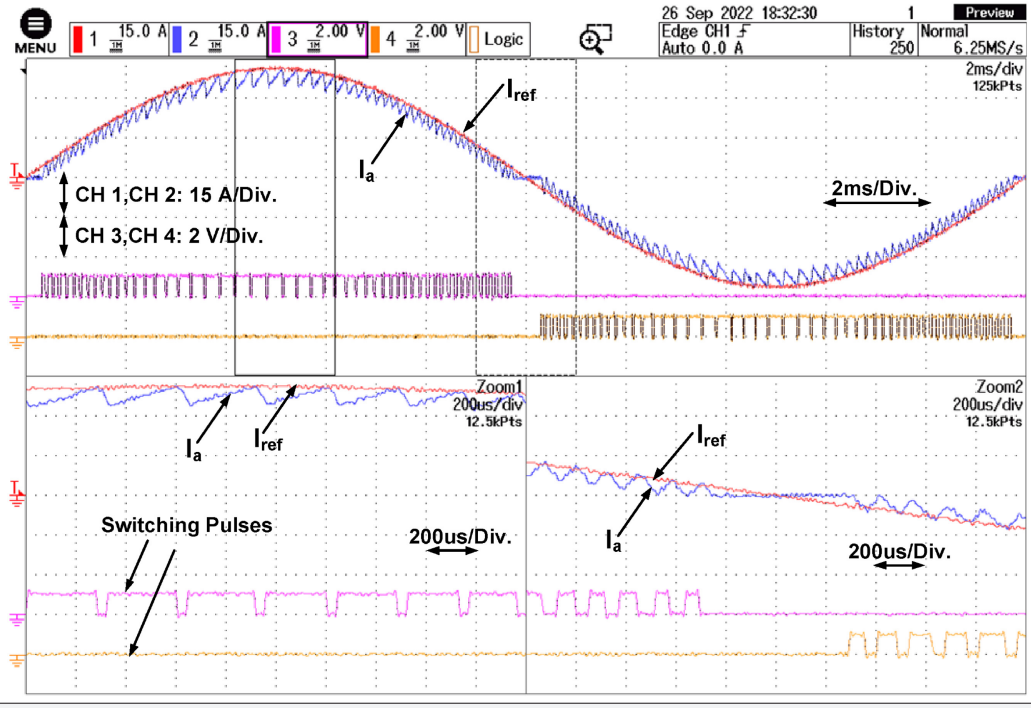

Fig. 13. Experimental results showing I_{ref}, I_a, and switching pulses for improved arithmetic optimization algorithm–revamped hysteresis current controller.

better efficiency of a converter, reduction of cooling parts, and high utilization of the device. Fig. 15 shows the current error of different schemes obtained from experimental results. The source current contains less harmonics in all the presented techniques as the current peaks are smaller.

VII. CONCLUSION

The objective of this article is to bring down the average switching losses and THD of source current to less than 5% at the common point of coupling satisfying the standard IEEE harmonic limits

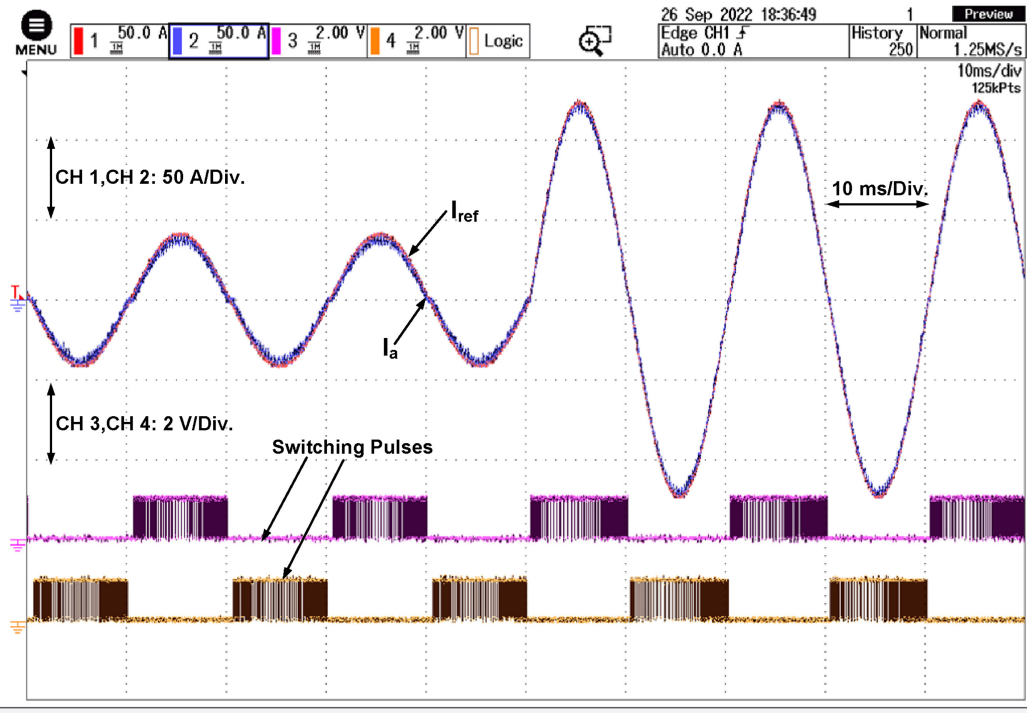

Fig. 14. Experimental results showing dynamic performance of I_{ref}, I_a, and switching pulses under step change in power from 1000 W to 2000 W for improved arithmetic optimization algorithm–revamped hysteresis current controller.

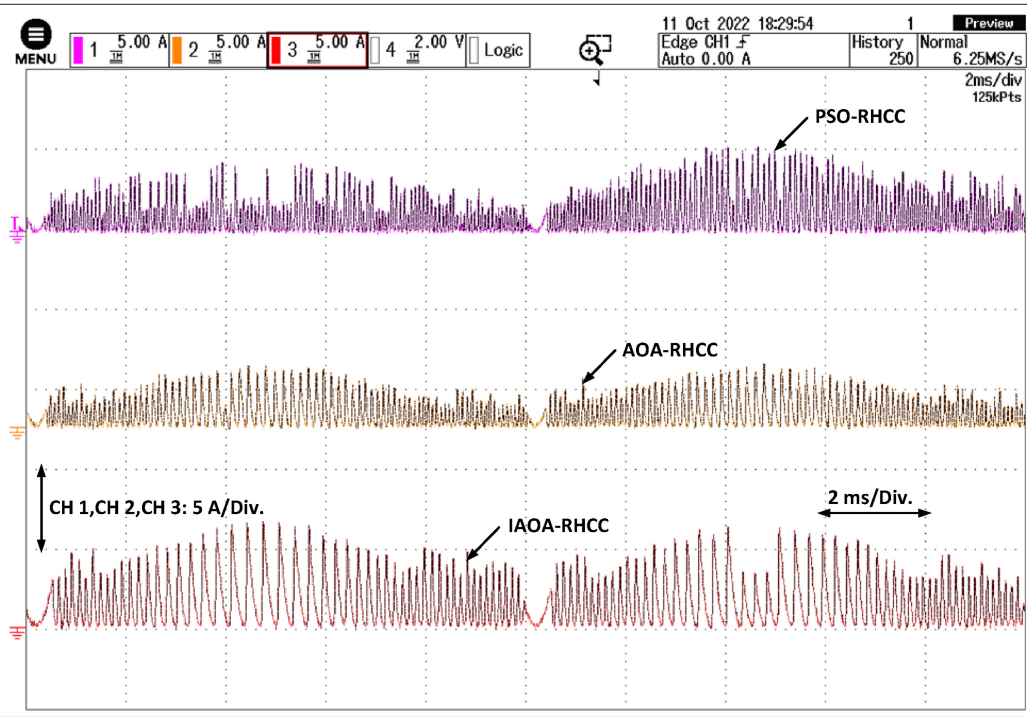

Fig. 15. Experimental results showing current error for (a) particle swarm optimization– revamped hysteresis current controller, (b) arithmetic optimization algorithm–revamped hysteresis current controller, and (c) improved arithmetic optimization algorithm–revamped hysteresis current controller.

519-1992, which is efficiently proven by the proposed technique. From a comprehensive simulation and experimental comparisons of the IAOA–RHCC technique with other techniques, the salient features of the proposed scheme can be summarized as follows: the steady-state performance of the IAOA–RHCC is superior to other schemes, the proposed technique achieves faster dynamic performance, the

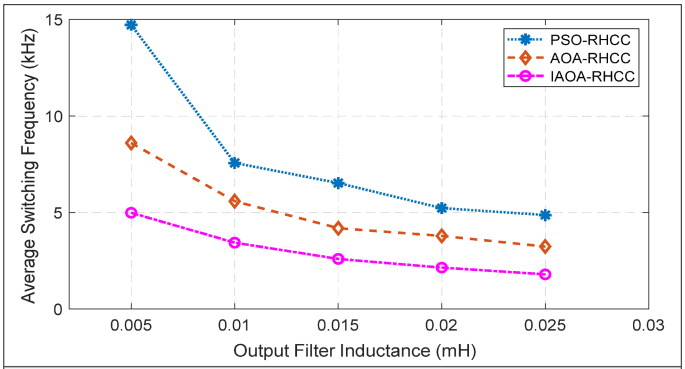

Fig. 16. Robustness of the proposed controller toward filter inductance variation at 5 mH, 10 mH, 15 mH, 20 mH, and 25 mH.

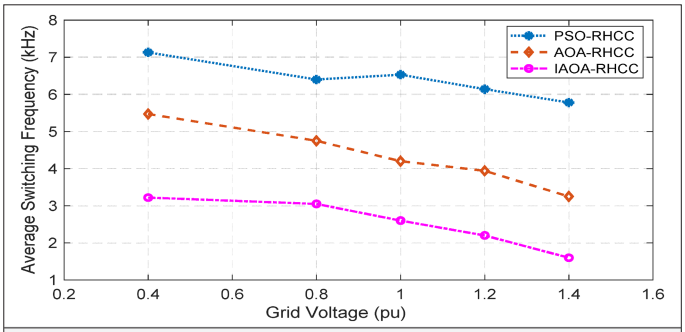

Fig. 17. Robustness of the proposed controller toward grid voltage variation at 40%, 80%, 100%, 120%, and 140% of grid voltage.

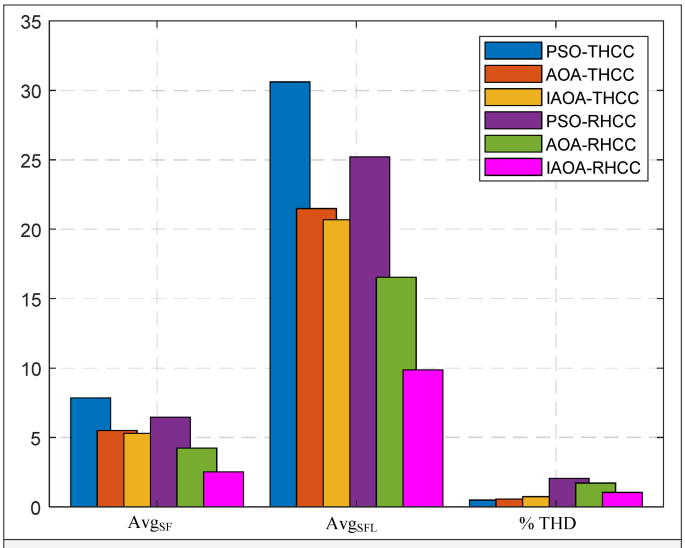

Fig. 18. Bar plot of various performance indices with different controllers.

convergence speed and exploitation capability are enhanced, the number of iterations for achieving the global optimum is lower for the IAOA–RHCC technique, the ASF and average switching losses are lesser in the IAOA–RHCC technique in comparison to THCCs. The results obtained from real-time OPAL RT support the MATLAB simulation results.

Peer-review: Externally peer-reviewed.

Author Contributions: Concept - B.M, B.K.S, S.P.; Design - B.M, B.K.S, S.P.; Supervision - B.K.S, S.P.; Data Collection and Processing - B.M, B.K.S, S.P.; Analysis and Interpretation - B.M, B.K.S, S.P.; Literature Review - B.M., S.P.; Writing - B.M., B.K.S.

Declaration of Interests: The authors have no conflicts of interest to declare.

Funding: The authors declared that this study has received no financial support.

REFERENCES

1. S. A. Aleem, S. M. S. Hussain, and T. S. Ustun, "A review of strategies to increase PV penetration level in smart grids," *Energies*, vol. 13, no. 3, p. 636, 2020. [CrossRef]
2. A. A. Estévez-Bén, A. Alvarez-Diazcomas, and J. Rodríguez-Reséndiz, "Transformerless multilevel voltage-source inverter topology comparative study for PV systems," *Energies*, vol. 13, no.12, p. 3261, 2020. [CrossRef]
3. P. C. Loh, M. J. Newman, D. N. Zmood, and D. G. Holmes, "A comparative analysis of multiloop voltage regulation strategies for single and three-phase UPS systems," *IEEE Trans. Power Electron.*, vol. 18, no. 5, pp. 1176–1185, 2003. [CrossRef]
4. S. Tahir, J. Wang, M. H. Baloch, and G. S. Kaloi, "Digital control techniques based on voltage source inverters in renewable energy applications: a review," *Electronics*, vol. 7, no. 2, p. 18, 2018. [CrossRef]
5. S. Chauhan, and G. Vashishtha, "Mutation-based arithmetic optimization algorithm for global optimization". *International Conference on Intelligent Technologies (CONIT)*, pp. 1–6, 2021. [CrossRef]
6. A. N. Tiwari, P. Agarwal, and S. P. Srivastava, "Performance investigation of modified hysteresis current controller with the permanent magnet synchronous motor drive," *IET Electr. Power Appl.*, vol. 4, no. 2, pp. 101–108, 2010. [CrossRef]
7. M. A. Elgendy, B. Zahawi, and D. J. Atkinson, "Assessment of perturb and observe MPPT algorithm implementation techniques for PV pumping applications," *IEEE Trans. Sustain. Energy*, vol. 3, no. 1, pp. 21–33, 2012. [CrossRef]
8. P. Suwannatrai, P. Liutanakul, and P. Wipasuramonton, "Maximum power point tracking by incremental conductance method for photovoltaic systems with phase shifted full-bridge dc-dc converter," In *Proceedings of the 8th Electrical Engineering/ Electronics, Computer, Telecommunications and Information Technology (ECTI) Association of Thailand-Conference, Khon Kaen, Thailand*, vol. 17–19, pp. 637–640, 2011. [CrossRef]
9. M. Lasheen, A. K. A. Rahman, M. Abdel-Salam, and S. Ookawara, "Performance enhancement of constant voltage based MPPT for photovoltaic applications using genetic algorithm," *Energy Procedia*, vol. 100, pp. 217–222, 2016. [CrossRef]
10. C. G. Villegas-Mier, J. Rodriguez-Resendiz, J. M. Álvarez-Alvarado, H. Rodriguez-Resendiz, A. M. Herrera-Navarro, and O. Rodríguez-Abreo, "Artificial neural networks in MPPT algorithms for optimization of photovoltaic power systems: A review," *Micro-Mach.*, vol. 12, no. 10, 2021. [CrossRef]
11. M. Premkumar, T. S. Babu, S. Umashankar, and R. Sowmya, "A new metaphor-less algorithms for the photovoltaic cell parameter estimation," *Optik*, vol. 208, p. 164559, 2020. [CrossRef]
12. D. A. Torrey, and A. M. A. M. Al-Zamel, "Single-phase active power filters for multiple nonlinear loads," *IEEE Trans. Power Electron.*, vol. 10, no. 3, pp. 263–272, 1995. [CrossRef]
13. H. Komurcugil, "Double-band hysteresis current-controlled single-phase shunt active filter for switching frequency mitigation," *Int. J. Electr. Power Energy Syst.*, vol. 69, pp. 131–140, 2015. [CrossRef]
14. J. Momin, and X. S. Yang, "A literature survey of benchmark functions for global optimization problems," *J. Math. Modell. Numer. Optim.*, vol. 4, no. 2, pp. 150–194, 2013.
15. C. Ammari, D. Belatrache, B. Touhami, and S. Makhloufi, "Sizing, optimization, control and energy management of hybrid renewable energy system-A review," *Energy Built Environ.*, pp. 2666–1233, 2021.
16. K. L. Du, and M. N. Swamy, "Particle swarm optimization," In *Search Optim. Meta-Heuristics*, pp. 153–173, 2016.
17. L. Abualigah, A. Diabat, S. Mirjalili, M. Abd Elaziz, and A. H. Gandomi, "The arithmetic optimization algorithm," *Comput. Methods Appl. Mech. Eng.*, vol. 376, p. 113609, 2021. [CrossRef]

18. S. A. S. Hasari, A. Salemnia, and M. Hamzeh, "Applicable method for average switching loss calculation in power electronic converters. Journal of Power Electronics," *Korean Power Electron. Soc.*, vol. 17, no. 4, pp. 1097–1108, 2017.

19. J. K. Singh, and R. K. Behera, "Hysteresis current controllers for grid connected inverter: Review and experimental implementation," In *Proceedings of the IEEE International Conference on Power Electronics, Drives and Energy Systems (PEDES)*, Chennai, India, 2018, pp. 1–6. [CrossRef]

Bhabasis Mohapatra completed his Bachelor of Technology from ITER, SOAU, Bhubaneswar. He completed his Masters of Technology in Power and Energy Systems from School of Electrical Engineering, KIITU, Bhubaneswar. He is currently pursuing his PhD at Siksha "O" Anusandhan (deemed to be) University in the Department of Electrical Engineering. He is currently working as a Faculty in Department of Electrical Engineering in SOADU, Bhubaneswar. His research area includes power quality issues, grid integration of renewable energy sources, evolving optimization techniques, and design of advanced controllers.

Binod Kumar Sahu received his bachelor's degree in Electrical Engineering from the Institution of Engineers, India, in 2001, his M.Tech. from NIT Warangal in 2003, and Ph.D from Siksha "O" Anusandhan (deemed to be) University in 2016. Presently, he is working as Professor in ITER, SOA (deemed to be) University, Bhubaneswar, Odisha, India. He is a member of IET and IEEE since 2014. His area of research interest includes automatic generation control, fuzzy logic-based control, time-series forecasting, and soft computing techniques.

Swagat Pati completed his Bachelor of Technology from ITER, Bhubaneswar. He completed his Masters of Research in Power Electronics and Drives from NIT, Rourkela. He was awarded his Ph.D. from Siksha O Anusandhan (deemed to be) University. Presently, he is working as Assistant Professor in Department of Electrical Engineering, ITER, Siksha O Anusandhan (deemed to be) University. His research area includes integration and power control of hybrid renewable energy systems, design of new topology for power electronic converters, electric drives application, and Flexible AC Transmission System (FACTS) devices.